Supporting Information

Artificial Interlayer Channels Composed of Brush-like Polymers: Enhanced Ion Transport of $Ti_3C_2T_x$ for Li Storage

Na Li,[‡a] Huihui An,[‡a] Yang Cheng,[a] Yuchen Duan,[a] Jiahao Li,[a] Jinwen Qin*[ab] and Minhua Cao*[a]

[a]Key Laboratory of Cluster Science, Ministry of Education of China, Beijing Key Laboratory of Photoelectronic/Electrophotonic Conversion Materials, School of Chemistry and Chemical Engineering, Beijing Institute of Technology, Beijing 100081, P. R. China

[b]Shandong Provincial Key Laboratory of Monocrystalline Silicon Semiconductor Materials and Technology, Dezhou University, Dezhou 253023, P. R. China

‡Contributed equally to this work

*Corresponding author: qjw@bit.edu.cn (J. Qin); caomh@bit.edu.cn (M. Cao)

1 Experimental Details

1.1 Synthesis of few-layer $Ti_3C_2T_x$ suspension

Typically, 0.998 g of lithium fluoride (LiF, 98%, Alfa Aesar) was added to 10 mL of hydrochloric acid (HCl, 12 M, Tianjin Fuyu Fine Chemical Co., Ltd), and the mixture was sealed and stirred. Subsequently, 1.0 g of Ti_3AlC_2 powder was dispersed slowly into the above mixture. The suspension was stirred for 24 h at 37 °C to remove Al layer of Ti_3AlC_2. Afterward, the multilayer $Ti_3C_2T_x$ product was washed with deionized water and centrifuged several times until the pH was approximately 7. Then, the as-obtained multilayer $Ti_3C_2T_x$ was redispersed into deionized water (20 mL) and sonicated for 1 h under N_2 in an ice-water bath. Finally, the few-layer $Ti_3C_2T_x$ suspension was collected after centrifugation at 3500 rpm for 50 min. For comparison, the pristine few-layer $Ti_3C_2T_x$ nanosheets were directly obtained via freezing-dry (FD-1-50, Beijing Bo medical Kang experiment Co., LTD).

1.2 Synthesis of $Ti_3C_2T_x$-PPM

The as-prepared few-layer $Ti_3C_2T_x$ suspension (50 mL, 2 mg mL^{-1}) was firstly sonicated for 30 min under N_2 in an ice-water bath. Then, 0.5 mL of poly(ethylene glycol) methyl ether acrylate monomer (PM, $(C_2H_4O)_9C_4H_6O_2$, TCI Shanghai) was dropped into the few-layer $Ti_3C_2T_x$ suspension, followed by stirring for 1 h. Subsequently, 20 mL of dilute nitric acid solution (1 M) containing 0.05 g of ammonium cerium nitrate ($Ce(NH_4)_2(NO_3)_6$, purity > 99.0%, Shanghai Aladdin Biochemical Technology Co., Ltd) was slowly added dropwise into the aforementioned mixture. After continuously stirring at room temperature for 6 h, the product was separated by centrifugation and washed several times with absolute ethanol and deionized water alternately to remove the redundant PM monomer and ammonium cerium nitrate. Finally, the product was collected and freeze-dried.

1.3 Synthesis of PPM

2 mL of PM monomer and 24 mg of $Ce(NH_4)_2(NO_3)_6$ were dissolved in 2 mL of HNO_3 (1 M) and mixed thoroughly. After polymerization, the product was washed three times with deionized water. Finally, the PPM polymer was dried in a vacuum

oven at 80 °C for 12 h.

1.4 Materials Characterizations

The crystal structure of the sample was determined using X-ray diffraction (XRD, Bruker D8 Advance) with the Cu−K_α radiation ($\lambda = 1.54056$ Å) in the range of 3 to 60° at a scan speed of 10° min^{-1}. Fourier transform infrared (FTIR) spectra were recorded on Bruker VECTOR 22. The morphologies of samples were characterized using field emission scanning electron microscopy (FE-SEM, Zeiss GeminiSEM 360). Nitrogen adsorption/desorption curves were measured by Brunauer-Emmett-Teller measurement to analyze the pore size distributions and surface area of the samples under N_2 physisorption at 77 K (KUBO-X1000). The content of PPM component in $Ti_3C_2T_x$-PPM was calculated based on thermogravimetric analysis (TGA) curve obtained by a thermogravimetric analyzer (DTG-60AH) in a N_2 atmosphere with a heating rate of 10 °C min^{-1} starting from room temperature. Inductively coupled plasma mass spectrometry (ICP-MS, JarrelASH) was used to analyze the composition of $Ti_3C_2T_x$-PPM.

1.5 Electrochemical measurements

The electrochemical measurements were carried out using standard CR2025 coin cells. Active materials, carbon black and poly(vinylidene fluoride) (PVDF, Shanghai Aladdin Biochemical Technology Co., Ltd) binder were mixed with a weight ratio of 7:2:1 using N-methyl-2-pyrrolidone (NMP, purity > 99.0%, Shanghai Aladdin Biochemical Technology Co., Ltd) as the solvent and pasted on the Cu foil to prepare the working electrode, followed by drying at 120 °C in a vacuum oven. The mass loading of the active materials was about 0.8-1.2 mg cm^{-2}. The working electrode was assembled with the lithium foil serving as both the reference and counter electrode to form the half-cell in an argon-filled glovebox. The electrolyte consists of a 1 M $LiPF_6$ in a 1:1:1 (vol%) mixture of ethylene carbonate (EC), diethyl carbonate (DEC) and ethyl methyl carbonate (EMC), with a Celgard 2400 membrane serving as the separator. Cyclic voltammetry (CV) curves were measured by a CHI-760E electrochemical workstation at various scan rates. The electrochemical impendence spectra (EIS) were performed with an amplitude of 5 mV in the frequency range from 100 kHz to 0.01 Hz. Galvanostatic discharge/charge profiles and the self-discharge testing were conducted on a LAND CT2001A. The EIS measurements and wide-temperature adaptability of cells were tested via a temperature chamber (Shenzhen Kejing Zhida Technology Co., LTD). The measurement procedures of self-discharge were as follows: the cells were charged to 3.0 V with the current densities of 0.1 and 1.0 A g^{-1} and then maintained at the desired voltage for 12 h before testing the open-circuit voltage. Galvanostatic intermittent titration technique (GITT) measurements were conducted using the LAND test system by discharging/charging for 20 min at a current density of 0.05 A g^{-1}. And the relaxation period was set as 2 h. For the Li-ion full cells, the cathode was made of commercial $LiFePO_4/LiNi_{0.8}Co_{0.1}Mn_{0.1}O_2$, carbon black, and PVDF in a weight ratio of 8:1:1 on an aluminum foil. The capacity ratio of anode/cathode was controlled to be around 1.2:1. Meanwhile, the anode and cathode were electrochemically activated for five cycles before they were used in the full cells. The test voltage was 0.5-3.9 V and the current density was 0.1-5.0 A g^{-1}. For the ex situ XRD experiments, the half cells were galvanostatically cycled at 0.1 A g^{-1} and then disassembled at various states of charging and discharging. Prior to conducting the ex situ XRD experiments, the electrodes were thoroughly washed with dimethyl carbonate (DMC) and dried overnight in vacuum.

2 Calculations

The ICP test was adopted to detect the concentrations of the Ti element in $Ti_3C_2T_x$ and $Ti_3C_2T_x$-PPM respectively. The content of PPM was calculated by the difference between the two. Specifically speaking, PPM content (W_{PPM}, wt %) in $Ti_3C_2T_x$-PPM was calculated using the following equation:

$$W_{PPM} = \frac{W_{TC} - W_{TC-PPM}}{W_{TC}} \tag{1}$$

where $W_{TC\text{-}PPM}$ (wt%) represents the Ti content in $Ti_3C_2T_x$-PPM, and W_{TC} (wt%) denotes the Ti content in $Ti_3C_2T_x$. Through the calculation, the PPM content in $Ti_3C_2T_x$-PPM was determined to be approximately 3.31 wt%.

To quantitatively distinguish the capacitive- and diffusion-controlled contributions, CV curves at a series of scan rates were tested. Generally, the relationship between the measured peak current (I_p) and scan rate (v) in a CV scan follows the formula:

$$I_p = av^b \tag{2}$$

$$\log\left(I_p\right) = \log\left(a\right) + b\log(v) \tag{3}$$

Apparently, the b value can be obtained by fitting slope of the log (I_p) *vs.* log (v) profile. When the b value is 0.5, it demonstrates a diffusion-controlled behavior, while the b value of 1.0 corresponds to a capacitive-controlled behavior. The capacitive- and diffusion-controlled contribution can be further quantitatively distinguished assuming that the current (I) is a combination of the capacitor- and diffusion-like controlled processes according to:

$$I = k_1 v + k_2 v^{1/2} \tag{4}$$

The frequencies of the Debye peak maxima, originated from the imaginary impedance as a function of frequency, is a characteristic frequency of the conductivity relaxation. There is a direct correlation between the Debye peak maxima and the reciprocal of the conductivity relaxation time (τ) or conductivity (σ):

$$2\pi f_{max} = \omega = (\tau)^{-1} = \sigma(e_0 \varepsilon')^{-1} \tag{5}$$

where ε' (real component of permittivity) is the frequency-independent permittivity, and e_0 is the permittivity of free space.

To calculate the Li^+ diffusion kinetics, a GITT test was conducted. The Li^+ diffusion coefficient (D_{Li^+}) was calculated according to the following equation:

$$D_{Li^+} = \frac{4}{\pi\tau} \times \left(\frac{m_B V_M}{M_B S}\right)^2 \times \left(\frac{\Delta E_s}{\Delta E_\tau}\right)^2 \tag{6}$$

where τ is pulse duration; m_B is the electrode active material mass; S is the geometric area of the Cu foil electrode; V_M is the molar volume, M_B is the molar mass; ΔE_s is the quasi-thermodynamic equilibrium potential difference before and after the current pulse; ΔE_τ is potential change during current pulse.

The calculation of apparent activation energy (E_a) is obtained by fitting the temperature-dependent EIS based on the following equations:

$$i = \frac{RT}{nFR_{ct}} \tag{7}$$

$$i = A\exp\left(-E_a/RT\right) \tag{8}$$

Here, A is the pre-exponential factor (the temperature-independent coefficient), R is the gas constant, T stands for the absolute temperature, n is the transferred electron number, F is the Faraday constant, and E_a is the apparent activation energy for ion migration.

The energy density (Wh kg^{-1}) and power density (W kg^{-1}) of the $LiFePO_4$‖$Ti_3C_2T_x$-PPM and $LiNi_{0.8}Co_{0.1}Mn_{0.1}O_2$‖$Ti_3C_2T_x$-PPM full cells were calculated according to the following equation:

$$Energy\ density\ (Wh\ kg^{-1}) = Discharge\ capacity\ (Ah\ kg^{-1}) \times\ Voltage\ (V) \tag{9}$$

$$Time\ for\ lithiation\ (h) = \frac{Discharge\ capacity\ (Ah\ kg^{-1})}{Current\ density\ (A\ kg^{-1})} \tag{10}$$

$$Power\ density\ (W\ kg^{-1}) = \frac{Energy\ density\ (Wh\ kg^{-1})}{Time\ for\ lithiation\ (h)} \tag{11}$$

3 Supplementary Figures

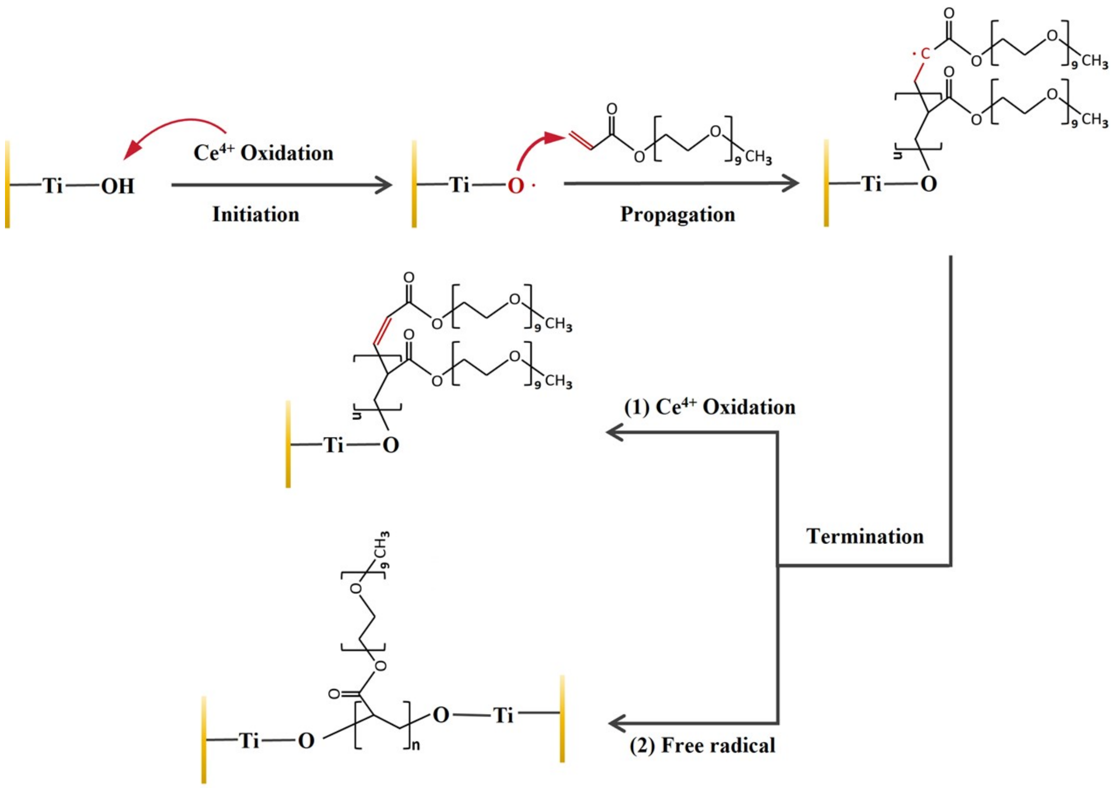

Fig. S1 Synthesis route of $Ti_3C_2T_x$-PPM through in situ polymerization.

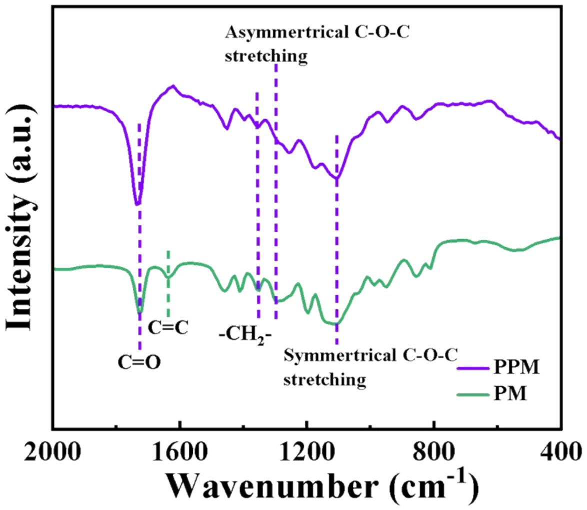

Fig. S2 FTIR spectra of PM and PPM.

For PPM sample, the characteristic band of the C=C bond in PM disappears, demonstrating the successful polymerization of PM to form PPM.[1, 2]

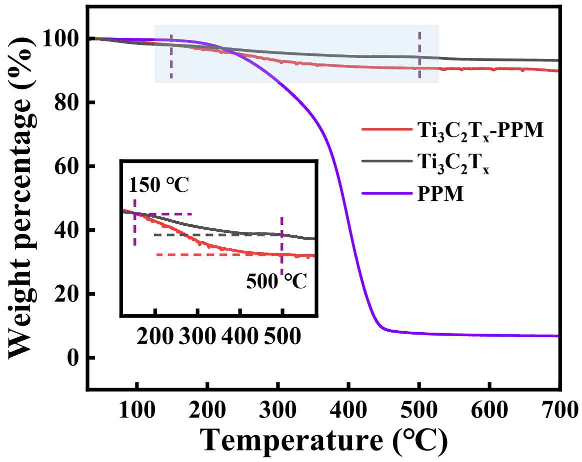

Fig. S3 TGA curves of $Ti_3C_2T_x$-PPM, $Ti_3C_2T_x$ and PPM.

PPM undergoes rapid decomposition within 150-500 °C and is fully degraded above 500 °C. Notably, $Ti_3C_2T_x$-PPM exhibits a mass loss trend identical to that of PPM in the 150-500°C range, confirming that the additional mass loss originated from the decomposition of interlayer PPM. Consequently, the PPM content in $Ti_3C_2T_x$-PPM can be quantitatively determined by calculating the difference between the residual mass percentages of $Ti_3C_2T_x$ (94.18 wt%) and $Ti_3C_2T_x$-PPM (90.54 wt%). The calculation results show that the mass percentage of PPM in $Ti_3C_2T_x$-PPM material is 94.18 wt% - 90.54 wt% = 3.64 wt%.

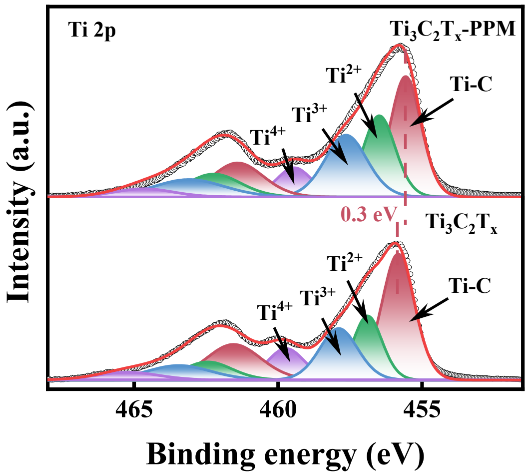

Fig. S4 Ti 2p XPS spectra of $Ti_3C_2T_x$-PPM and $Ti_3C_2T_x$.

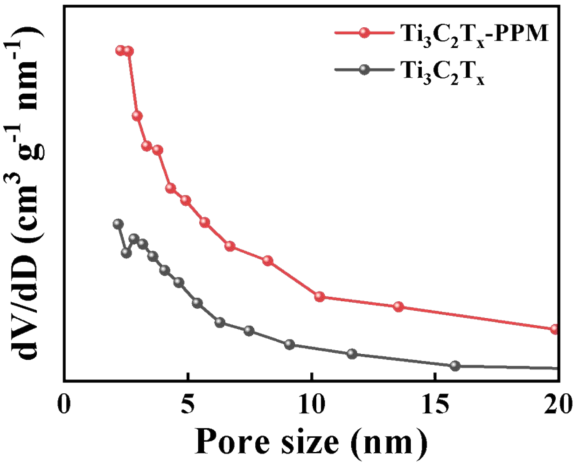

Fig. S5 Pore size distribution curves of $Ti_3C_2T_x$-PPM and $Ti_3C_2T_x$.

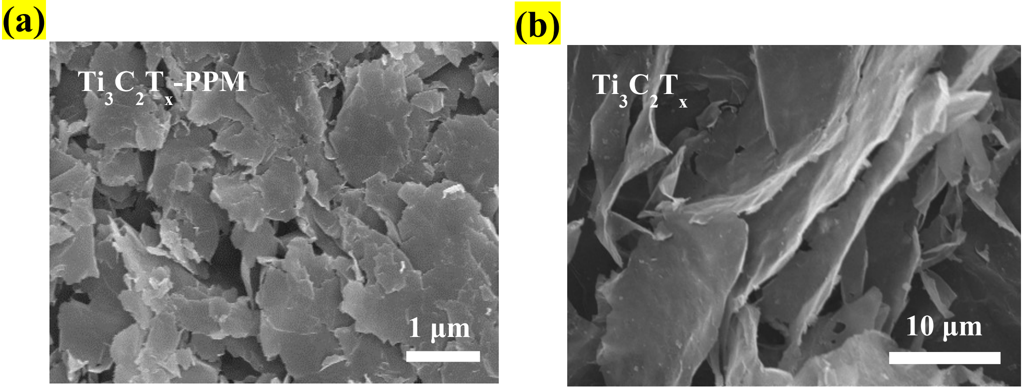

Fig. S6 (a) High-magnification FE-SEM image of $Ti_3C_2T_x$-PPM. (b) Low-magnification FE-SEM image of $Ti_3C_2T_x$.

As a result of the self-restacking of $Ti_3C_2T_x$ nanosheets through van der Waals forces, the formation of large-size $Ti_3C_2T_x$ structures with the parallel arrangement can be observed.

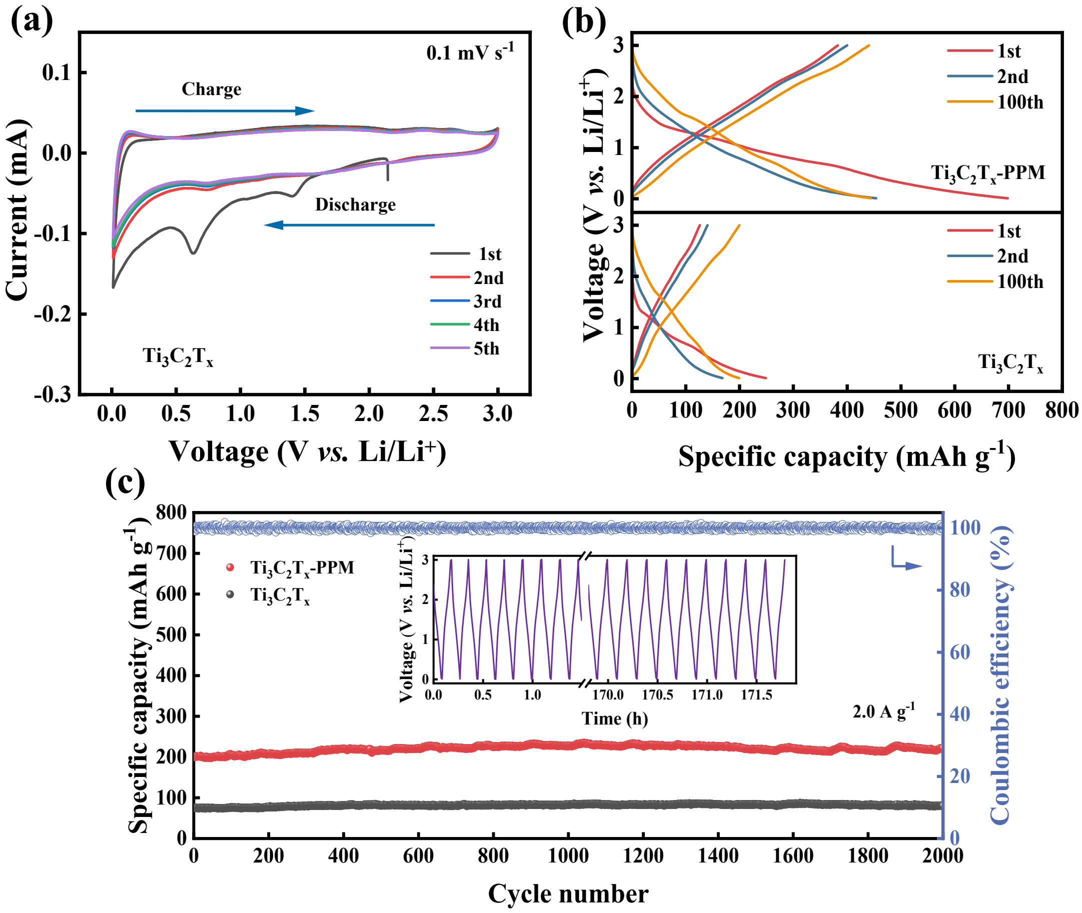

Fig. S7 (a) The initial three CV cycles of $Ti_3C_2T_x$ at 0.1 mV s^{-1}. (b) GCD curves of $Ti_3C_2T_x$-PPM and $Ti_3C_2T_x$ at 0.1 A g^{-1}. (c) Long-term cycling performances of $Ti_3C_2T_x$-PPM and $Ti_3C_2T_x$ at 2.0 A g^{-1} (insets: time-voltage curves for the first and last 10 cycles).[3, 4]

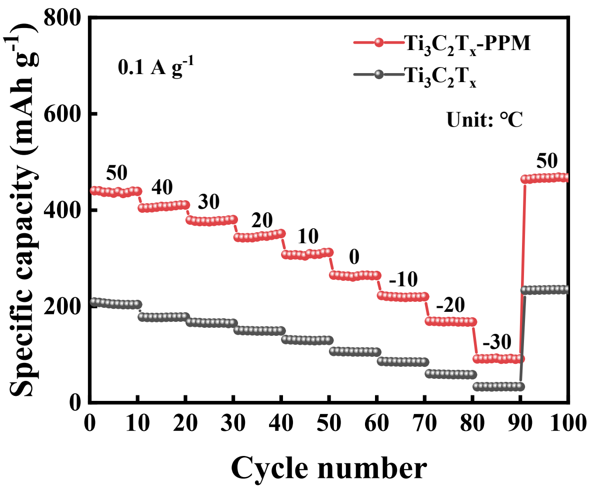

Fig. S8 Cycling performances of $Ti_3C_2T_x$-PPM and $Ti_3C_2T_x$ over the temperature range of 50 to -30 °C.

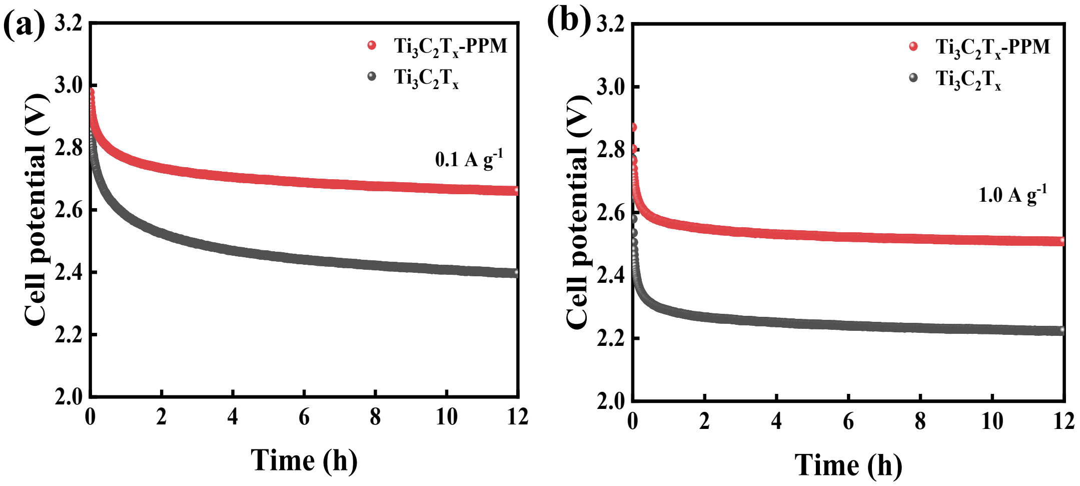

Fig. S9 Self-discharge testing of $Ti_3C_2T_x$-PPM and $Ti_3C_2T_x$ after being charged at current densities of (a) 0.1 A g^{-1} and (b) 1.0 A g^{-1}.

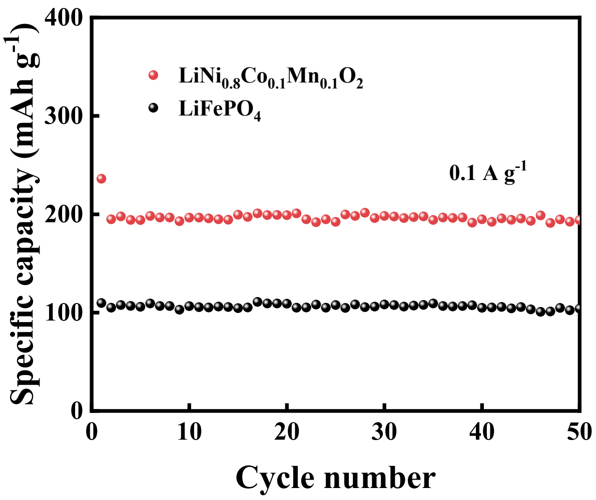

Fig. S10 Cycling performances for $LiNi_{0.8}Co_{0.1}Mn_{0.1}O_2$ and $LiFePO_4$ in half cells.

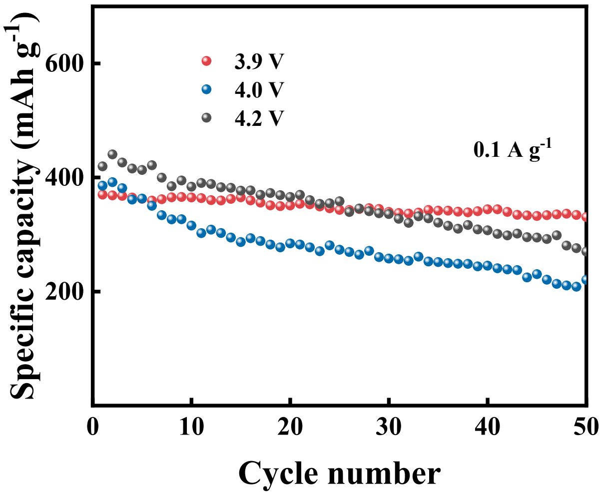

Fig. S11 Cycling performances of $LiNi_{0.8}Co_{0.1}Mn_{0.1}O_2\|Ti_3C_2T_x$-PPM under different cut-off voltages.

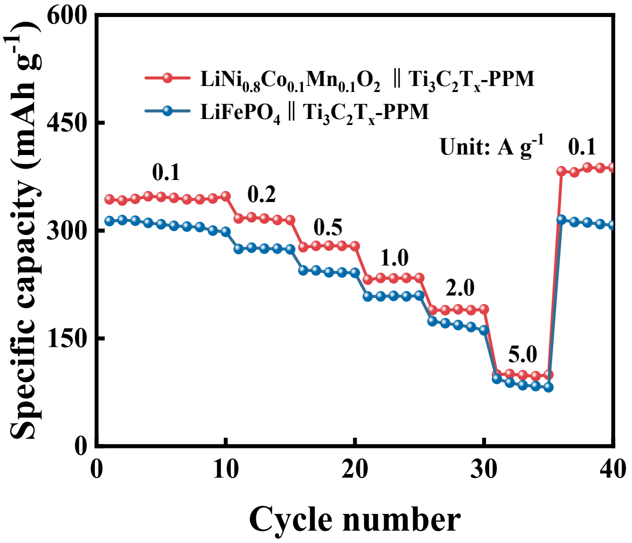

Fig. S12 Rate capabilities of $LiFePO_4$ ‖ $Ti_3C_2T_x$-PPM and $LiNi_{0.8}Co_{0.1}Mn_{0.1}O_2$ ‖ $Ti_3C_2T_x$-PPM full cells.

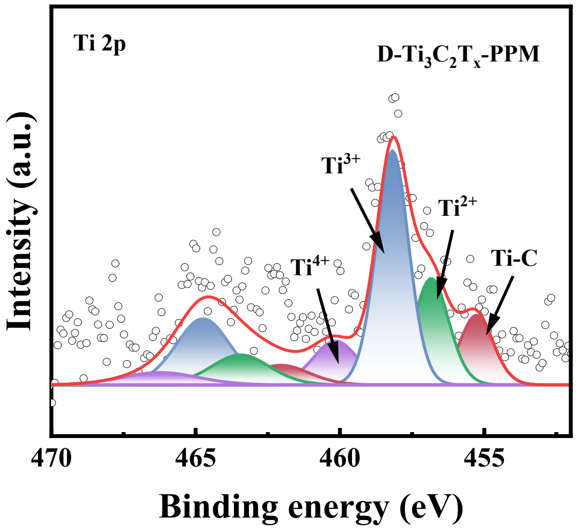

Fig. S13 Ti 2p XPS spectrum of D-$Ti_3C_2T_x$-PPM.

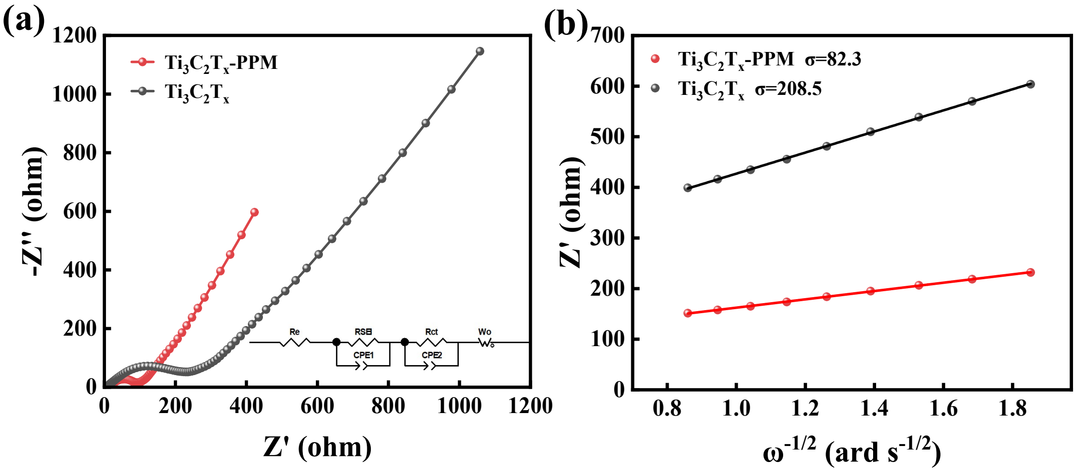

Fig. S14 (a) Nyquist plots for $Ti_3C_2T_x$-PPM and $Ti_3C_2T_x$ (inset: equivalent circuit). (b) Linear relationship between Z and $\omega^{-1/2}$ in the low-frequency region.

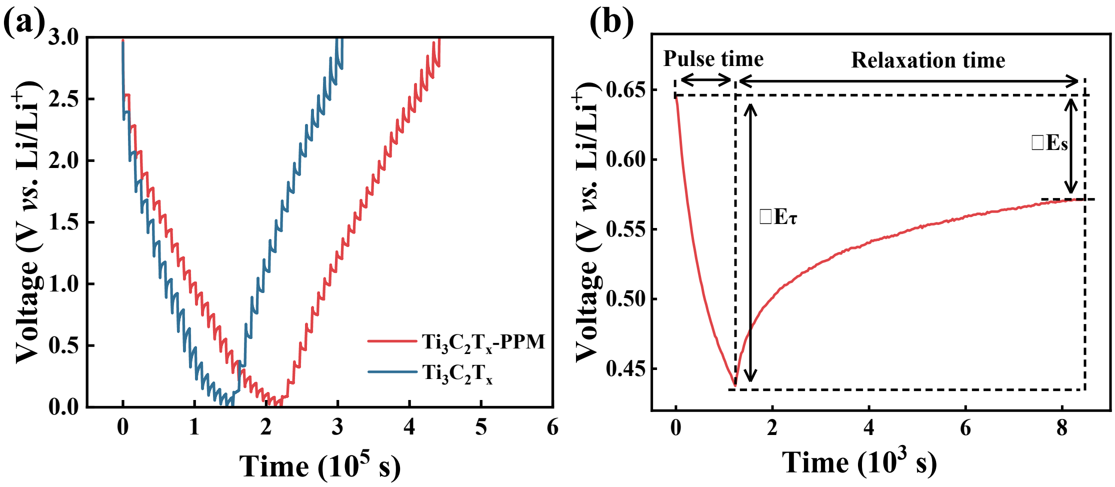

Fig. S15 (a) GITT curves for $Ti_3C_2T_x$-PPM and $Ti_3C_2T_x$. (b) Time *vs.* voltage profile of single titration of $Ti_3C_2T_x$-PPM.

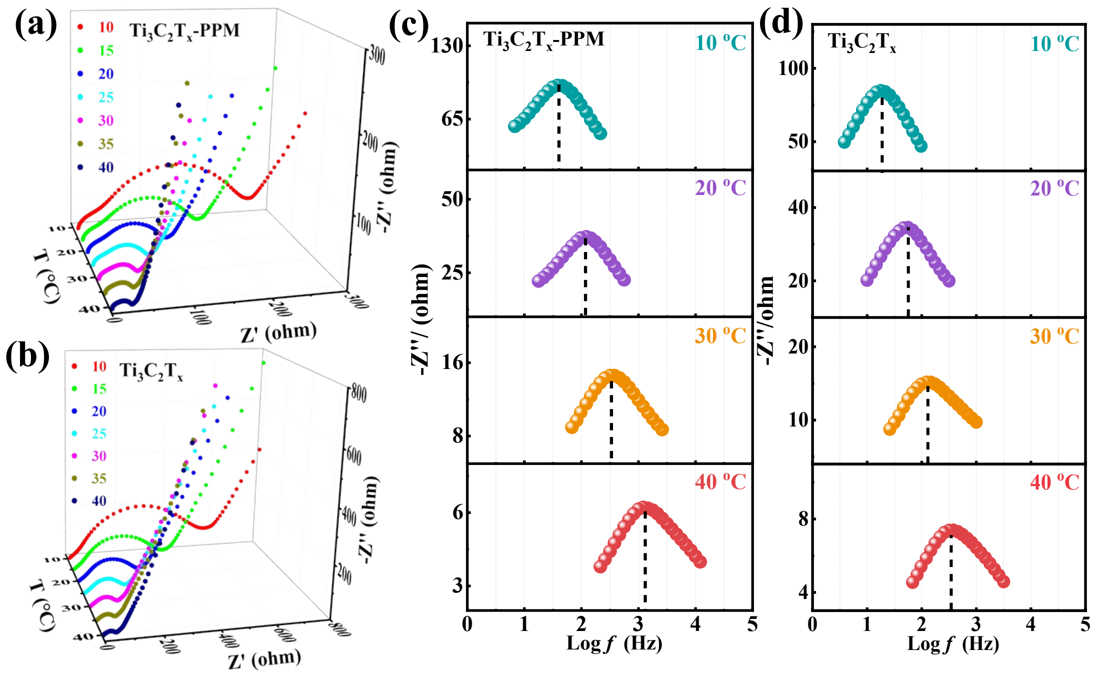

Fig. S16 Temperature-dependent Nyquist plots and corresponding Debye plots of (a, c) $Ti_3C_2T_x$-PPM and (b, d) $Ti_3C_2T_x$.

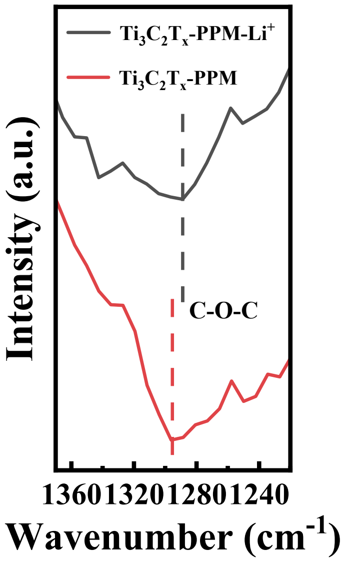

Fig. S17 FTIR spectra of $Ti_3C_2T_x$-PPM-Li^+ and $Ti_3C_2T_x$-PPM.

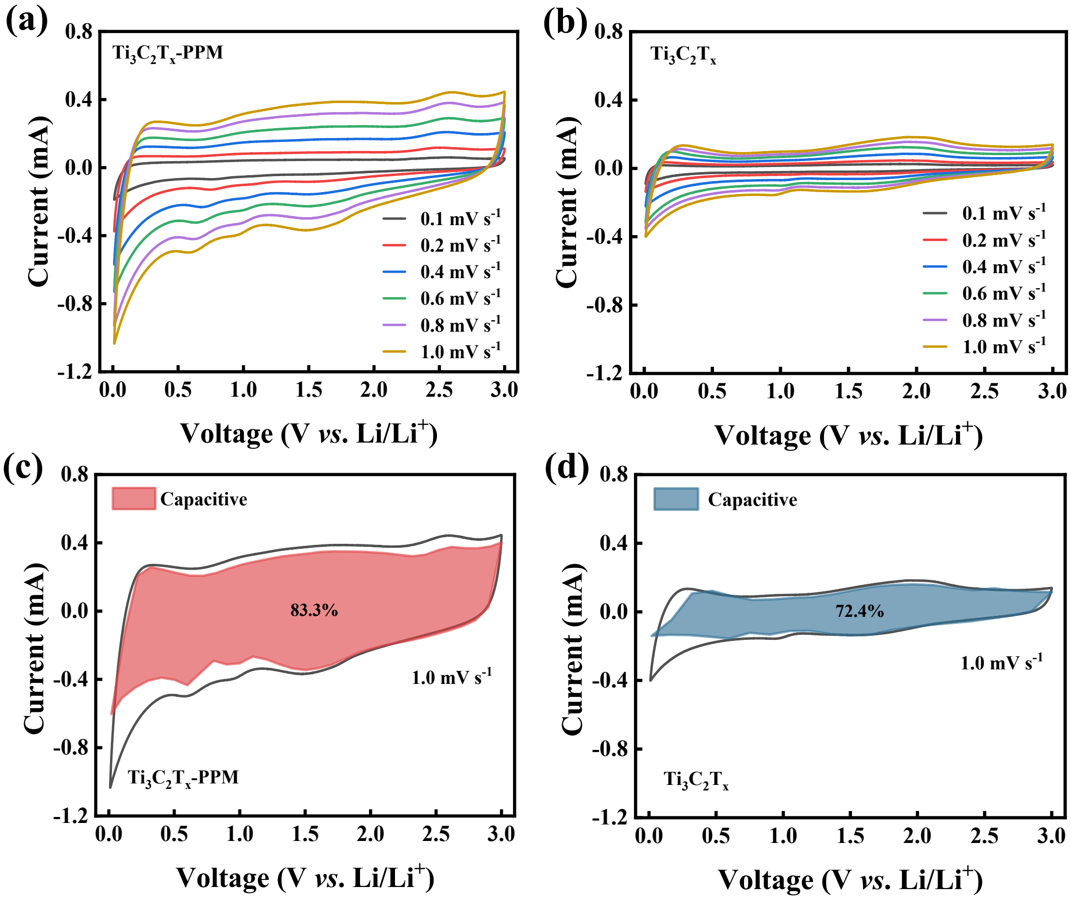

Fig. S18 CV curves of (a) $Ti_3C_2T_x$-PPM and (b) $Ti_3C_2T_x$ at different scan rates. Capacitive contribution of (c) $Ti_3C_2T_x$-PPM and (d) $Ti_3C_2T_x$ at 1.0 mV s^{-1}.

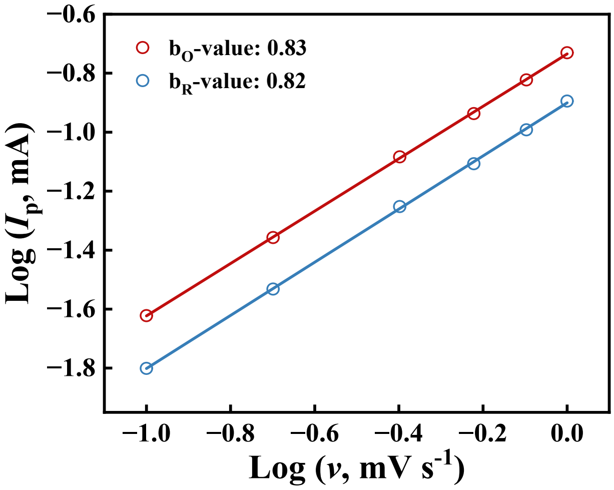

Fig. S19 Linear relationship between log (I_p) and log (v) of $Ti_3C_2T_x$.

Table S1 The Ti contents in $Ti_3C_2T_x$ and $Ti_3C_2T_x$-PPM determined by ICP analysis.

Sample	W_{Ti} (wt%)
$Ti_3C_2T_x$	26.26
$Ti_3C_2T_x$-PPM	25.39

Table S2 Calculated R_{ct} and σ values for $Ti_3C_2T_x$-PPM and $Ti_3C_2T_x$.

Sample	R_{ct} (ohm)	σ
$Ti_3C_2T_x$-PPM	62.9	82.3
$Ti_3C_2T_x$	149.5	208.5

References

1 D. J. Lv, Q. J. Li, P Wu, X. L. Zhang, L Wang, B Li, N Gao, Z. S. Liu and L. P. Wang. *Langmuir*, 2024, **40**, 11287–11296.

2 Q. Y. Li, B Li, D. J. Lv, P Wu, Q. W. Tang, T. Y. Zhang, S Jiang and N Zhang. *Phys. Chem. Chem. Phys.*, 2023, **25**, 31178.

3 S. Zhao, X. Meng, K. Zhu, F. Du, G. Chen, Y. Wei, Y. Gogotsi and Y. Gao, *Energy Storage Mater.*, 2017, **8**, 42-48.

4 G. Zou, Z. Zhang, J. Guo, B. Liu, Q. Zhang, C. Fernandez and Q. Peng, *ACS Appl. Mater. Interfaces*, 2016, **8**, 22280-22286.